



Synthesis and characterization of a nanoadsorbent for removal of bisphenol A by hydrous magnesium oxide: kinetic and isotherm studies

P. Bahrami^a, I. Kazeminezhad^{b,c}, Z. Noorimotlagh^d, S.S. Martinez^e, M. Ahmadi^{a,d}, M. Saraji^f, M. Ravanbakhsh^a, N. Jaafarzadeh^{a,d,*}

^aDepartment of Environmental Health Engineering, Ahvaz Jundishapur University of Medical Sciences, Ahvaz, Iran, emails: p.bahrami60@yahoo.com (P. Bahrami), mapseh@gmail.com (M. Ravanbakhsh)

^bDepartment of Physics, Faculty of Science, Shahid Chamran University of Ahvaz, Ahvaz, Iran, email: i.kazeminezhad@scu.ac.ir

^cCenter for Research on Laser and Plasma, Shahid Chamran University of Ahvaz, Ahvaz, Iran

^dEnvironmental Technologies Research Center, Ahvaz Jundishapur University of Medical Sciences, Ahvaz, Iran,

Tel./Fax: +98 6133738485, +98 6133738484; emails: jaafarzadeh-n@ajums.ac.ir (N. Jaafarzadeh),

noorimotlagh.zahra@gmail.com (Z. Noorimotlagh), ahmadi241@gmail.com (M. Ahmadi)

^eCentro de Investigación en Ingeniería y Ciencias Aplicadas, Av. Universidad 1001, Col. Chamilpa, Cuernavaca, Morelos, Mexico, email: ssilva@uaem.mx

^fDepartment of Chemistry, Isfahan University of Technology, Isfahan, Iran, email: saraji@cc.iut.ac.ir

Received 13 July 2017; Accepted 24 January 2018

ABSTRACT

Endocrine-disrupting chemicals, bisphenol A (BPA), are currently unregulated chemicals that interfere with the endocrine systems of organisms by different ways. The removal of BPA in this study is by its adsorption on hydrous magnesium oxide (HMgO) nanoparticles synthesized by the sol-gel method via 1-*n*-butyl-3-methylimidazolium tetrafluoroborate ionic liquid. Several analytical techniques such as scanning electron microscopy, X-ray diffractometer (XRD) and Fourier transform infrared spectroscopy were used to characterize HMgO nanoparticles. The influence of different experimental factors including solution pH, contact time, adsorbent dosages, initial BPA concentrations and regeneration was studied. The XRD analysis showed that HMgO nanoparticles were successfully synthesized and illustrated their purity and crystallinity. Findings revealed that BPA removal was decreased from 4.2 to 2.5 mg/g by an enhancement in solution pH from 9 to 11, respectively. Increasing adsorbent dosage from 2 to 100 mg/L resulted in increasing the removal from 24.9% to 100%, respectively. In addition, 4.2 mg/g and 50 min were respectively obtained as the adsorption capacity and equilibrium reaction time of BPA adsorption in aqueous media using HMgO. Findings of equilibrium and kinetic studies revealed higher ability of Freundlich isotherm ($R^2 = 0.997$) and pseudo-first-order kinetic ($R^2 = 0.998$) models, than the other models for fitting the data of BPA adsorptive removal. Furthermore, it can be concluded that HMgO nanoparticles were the appropriate sorbents to remove BPA from aqueous media.

Keywords: Sol-gel process; Magnesium oxide; Bisphenol A; Adsorption; Isotherm; Kinetic

1. Introduction

Nowadays, a wide variety of hazardous organic compounds such as perfluorooctane sulfonic acid and its

derivatives, polychlorinated biphenyls, polycyclic aromatic hydrocarbons and endocrine-disrupting chemicals (EDCs) in the environment are widespread, due to the extensive use of development of chemical industries [1–7]. The presence of these pollutants in aquatic environments is a significant and critical topic, due to their toxicity [8,9]. EDCs are chemicals,

* Corresponding author.

currently unregulated, that interfere with the endocrine systems of organisms by different ways [10–12].

Bisphenol A (BPA), one of these EDCs, is a xenobiotic compound and a great public health concern which was extensively used in a range of applications, including as an intermediate for the production of pesticides, epoxy resins, polycarbonate plastic, packaging, canned foods and beverages, dish and laundry detergents, sunscreen lotions, body wash/lotions, bar soaps, shampoo, conditioners, shaving creams, toys, textiles and leathers [2,8,9,13,14]. BPA has unique and excellent characteristics such as solid form at room temperature, low vapor pressure and volatility and moderate water solubility [9]. Several studies have reported that BPA exhibits weak estrogen-like properties using *in vitro* and *in vivo* bioassays [15]. It has been reported that the exposure to very low BPA levels may cause hormone-dependent cancer, adversarial effects on the reproduction, inducing oxidative stress and apoptosis [14,16–23]. Therefore, degradation of the hormone-like materials in water resources, because of their negative effects on human health, is of great importance.

Recently, various removal methods have been used for removing BPA from different sample matrices, including physical, chemical and biological technologies (e.g., adsorption, biological treatment, ozonation, UV radiation, chemical coagulation–flocculation, photocatalytic degradation and membrane separation) [2,14,24–33]. Among these methods, adsorption has been widely applied, because of its cost-effectiveness, high efficiency, simple design procedure, production of insignificant amounts of residual materials, and fewer harmful secondary products [2,8,14,15,24,25,34]. During the last decades, a considerable attention has been paid for utilization of various metal oxides as adsorbents [25]. Among all metal oxides, hydrous magnesium oxide (HMgO) with strong basic properties are known as an adsorbent material, due to its high removal efficiency, lower cost, high surface reactivity, non-toxicity, chemical stability and ease of production [25,35]. Nowadays, nanomaterials have received significant attentions, due to their high surface area, the presence of large numbers of active sites and high stability, compared with the most traditional adsorbents [24,25,36–39]. Therefore, various methods have been adopted for the synthesis of MgO nanoparticles such as sol–gel method, precipitation, hydrothermal and chemical vapor deposition [35,40]. Among these methods sol–gel technique is undoubtedly the simplest and cheapest method, synthesize in low temperature, control on the size and shape of nanoparticles as well as production of nanopowders with high purity [41,42]. In the present paper, HMgO nanoparticles were synthesized by sol–gel method using imidazolium based ionic liquid [BMIM] BF⁴⁻. The influence of different experimental factors such as solution pH, contact time, adsorbent dosages, initial BPA concentrations and regeneration was studied. Furthermore, the experimental data were fitted to some equilibrium and kinetic models to find the adsorption mechanism.

2. Experimental

2.1. Materials

Magnesium nitrate (Mg(NO₃)₂·6H₂O), sodium hydroxide solution (NaOH), hydrochloric acid (HCl), 1-*n*-butyl-3-methylimidazolium tetrafluoroborate

([BMIM] BF⁴⁻), methanol (CH₃OH), acetic anhydride (C₄H₆O₃), sodium carbonate (Na₂CO₃), dichloromethane (CH₂Cl₂), methylene blue (C₁₆H₁₈ClN₃S) and acetonitrile (C₂H₃N) were purchased from Merck Co. (Darmstadt, Germany) and BPA from Khuzestan Petrochemical Company (Iran), respectively. All the reagents were of analytical grade and used without further purification. The chemical structure of the BPA (synonym: 2,2-bis(4-hydroxyphenyl)propane and 4,4'-isopropylidenediphenol, chemical formula: C₁₅H₁₆O₂ and molecular weight (g/mol): 228.29) is shown in Fig. 1. A stock solution of BPA (500 ppm) was prepared by dissolving BPA in ethanol. The stock solution was diluted with different amounts of deionized water to prepare desired concentrations of BPA solution.

2.2. Synthesis of HMgO nanostructures (adsorbent)

Hydrous magnesium oxide nanoparticles were synthesized through sol–gel method using 1-*n*-butyl-3-methylimidazolium tetrafluoroborate ionic liquid, as explained by Sundrarajan et al. [43] and Meenakshi et al. [44]. Initially, 6.4075 g Mg(NO₃)₂ was added into the 50 mL H₂O₂ solution and 1 mL [BMIM] BF⁴⁻. The solution was sealed immediately and stirred rapidly using a magnetic stirrer for 15 min to obtain homogeneous solution and until the magnesium nitrate was fully dissolved. Then, 30 mL of 1 M NaOH solution was slowly added dropwise into the above resulting solution under continuous stirring. This would result in the hydrolysis of magnesium nitrate which is indicated by the appearance of turbidity in the solution leading to the formation of HMgO in the form of gel. After completion of this whole reaction process, the resulting solution was stirred overnight at room temperature which was then centrifuged (3,000 rpm – 15 min), washed with deionized water and dried at 80°C for 1 h, manually ground and calcined in a muffle furnace (FP125 model) at 300°C for 2 h to give pure HMgO nanoparticles.

2.3. Characterization

MgO nanoparticles were characterized by X-ray diffractometer (XRD) with Cu Kα (λ = 1.54056 Å) radiation on a Philips Xpert diffractometer (USA). The morphology was analyzed by scanning electron microscopy (SEM) using a Philips XL30 (USA). The accelerating voltage and applied current were 40 kV and 30 mA, respectively. The pore size diameter of HMgO nanoparticles was measured using Measure IT and Nano Measurement software taken via SEM image. Fourier transform infrared spectroscopic (FTIR) spectra were recorded using a spectrophotometer (Spectrum RX I, PerkinElmer, USA). The spectra were recorded from 4,000 to 500 cm⁻¹ at a resolution of 1 cm⁻¹ and are baseline corrected. The adsorbed amount of methylene blue on the

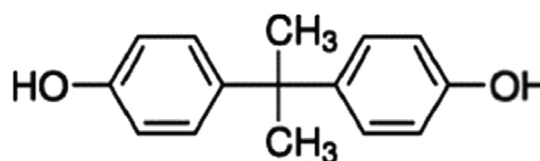


Fig. 1. Chemical structure of bisphenol A (BPA).

surfaces of adsorbent was considered 130 \AA^2 ($1 \text{ \AA} = 0.1 \text{ nm}$) which assumed as specific surface area [45]. Moreover, pH drift approach was used for measuring point of zero charge (pH_{pzc}) and the adsorbent surface charge [46]. A metrohm pH-meter (Model: AZ, Horiba D-14, Kyoto, Japan) was used for the measurement of solution pH. The concentration of the residual BPA was measured by a gas chromatography (GC Agilent 7890 model, USA) with a DB-5 column (0.25 \mu m phase, 0.25 mm i.d., 30 m flow rate of 1 mL/min of the carrier gas (helium)) with increasing from 50°C to 300°C at 10°C/min , and then kept for 2 min at 300°C .

2.4. BPA adsorption experiments

The adsorptive removal of BPA in aqueous media was studied in batch experiments at room temperature (25°C). In this regards, the specific adsorbent dosages were added to 100 mL BPA solutions with different concentrations and shaken vigorously on a rotary shaker at different time periods. In this study, various factors have been investigated such as, contact time ($5\text{--}200 \text{ min}$), solution pH ($4\text{--}11$), adsorbent dosages ($2\text{--}100 \text{ mg/L}$), its adsorption and desorption, and initial BPA concentrations of $2\text{--}200 \text{ mg/L}$. Batch experiments of BPA removal were carried out twice and the mean values of data were considered as final results. In addition, HCl and NaOH solutions were used for adjusting solution pH.

2.5. Adsorption isotherms

The experimental equilibrium data were fitted to the Freundlich (Eq. (1)), Langmuir (Eq. (2)), Dubinin–Radushkevich (D–R) (Eqs. (3) and (4)), Redlich–Peterson (R–P) (Eq. (5)), Temkin (Eq. (6)) and Langmuir–Freundlich (Eq. (7)) isotherm models expressed by the following equations:

$$\text{Log}q_e = \text{Log}K_f + \frac{1}{n}\text{Log}C_e \quad (1)$$

where K_f (L/g) and n are the constants of model, indicating adsorption capacity and intensity, respectively. These parameters were respectively obtained through the intercept and slope of plot $\text{ln}q_e$ against $\text{ln}C_e$, as follows [47–49]:

$$\frac{C_e}{Q_e} = \frac{1}{bQ_m} + \frac{C_e}{Q_m} \quad (2)$$

where C_e (mg/L) expresses the concentration of BPA at the equilibrium time and b (L/mg) is the model constant. Q_e (mg/g) and Q_m (mg/g) are the sorption capacity of the adsorbent and the maximum monolayer adsorbent capacity at the equilibrium time, respectively. The slope and intercept of plot C_e/q_e vs. C_e were used for obtaining Q_m and b as follows [47–49]:

$$\text{ln}Q = \text{ln}Q_0 - k\varepsilon^2 \quad (3)$$

where Q is the concentration of adsorbed BPA (mol/g), Q_0 (mol/g) is the adsorption capacity and k (mol^2/J^2) is the

constant attributed to the adsorption energy, respectively [45–47]. Besides, ε is the Polanyi potential (J^2/mol^2) that was determined as follows:

$$\varepsilon = RT \ln \left(1 + \frac{1}{C_0} \right) \quad (4)$$

where R is the universal gas constant (8.314 J/mol K) and T (K) is the temperature of the solution containing adsorbate molecules, respectively [47–49].

$$\ln \left(K_R \frac{C_e}{q_e} - 1 \right) = \ln(a_R) + \beta \ln(C_e) \quad (5)$$

where K_R is the R–P constant (L/g), a_R is the R–P constant (L/mg) and β is the exponent which lies between 1 and 0 [45].

$$q_e = \frac{RT}{b} \ln K_i + \frac{RT}{B} \ln C_e \quad (6)$$

where K_i is the equilibrium binding constant (L/mol) corresponding to the maximum binding energy, b is related to the adsorption heat, R is the universal gas constant (8.314 J/K mol) and T is temperature (K) [45].

$$q = \frac{(K_a C_{\text{eq}})^n Q_m}{(K_a C_{\text{eq}})^n} \quad (7)$$

where q is the amount of BPA adsorbed on the HMgO nanoparticles at equilibrium (mg BPA/g HMgO), Q_m is the adsorption capacity of the system (mg of sorbate/g sorbent), which can also be expressed as N_s , which is a measure of total number of binding sites available per gram of sorbent, C_{eq} is the aqueous phase concentration at equilibrium (mg/L), K_a is the affinity constant for adsorption (L/mg) and n is the index of heterogeneity [45].

2.6. Kinetic studies

Pseudo-first-order and pseudo-second-order models were used for understanding the adsorption mechanism. The linearized-integral form of the pseudo-first-order model is given as follows:

$$\ln(q_e - q_t) = \ln q_e - k_1 t \quad (8)$$

where q_e and q_t (mg/g) represent the adsorbed quantities of BPA at equilibrium and specific time periods, respectively. Furthermore, k_1 and t are the specific rate constant of model and time (min), respectively. k_1 and q_e were also obtained by the slope and intercept of plot $\ln(q_e - q_t)$ vs. time (t), respectively. Eq. (9) shows the linear form of pseudo-second-order kinetic model as follows:

$$\frac{t}{q_t} = \frac{1}{k_2 q_e^2} + \frac{t}{q_e} \quad (9)$$

where k_2 is defined as the specific rate constant of pseudo-second-order kinetic model. While, the rest of parameters were defined above. The intercept and slope of plot t/q_e vs. time (t) were used for obtaining the amount of k_2 and q_e respectively [47–50].

3. Results and discussion

3.1. Characterization of HMgO nanoparticles

The SEM image was taken to investigate the surface properties and the structure of prepared HMgO (Fig. 2(a)). Fig. 2(a) shows the SEM image of HMgO nanoparticles taken at different magnifications. SEM micrograph showed that HMgO nanoparticles size is in the range of 20–80 nm. As shown in Fig. 2(a), the synthesized MgO have the cubic and hexagonal structure, condensed and without pores. Ionic liquid has a very important role in the formation of nanoparticles. Besides, the results of the specific surface area analysis by methylene blue molecules exhibited a specific surface area of 173 m²/g for HMgO nanoparticles prepared via sol–gel process, which revealed proper surface area for adsorption of BPA molecules [43,44]. X-ray diffraction pattern was employed for investigation of the crystalline phase and structure of prepared HMgO nanoparticles. Fig. 2(b) exhibits the XRD pattern of the calcined products at 300°C and in a 2θ range of 10°–85°. It also shows the partial crystalline nature. Clearly, the characteristic diffraction peaks of the XRD pattern for HMgO sample at 18.62, 37.93, 50.97, 58.76, 62.26, 68.45, 72.03 and 81.50 were attributed to the (001), (101), (102), (110), (111), (103), (112) and (202), respectively, which was in agreement with the 00-002-1092 standard card from Joint Committee on Powder Diffraction Standards (JCPDS). The average crystallite size of HMgO nanoparticles was determined by Debye–Scherer formula as follows:

$$D = \frac{K\lambda}{\beta \cos\theta} \quad (10)$$

where K (0.94) is a shape factor, λ is the wavelength of Cu $K\alpha$ radiation ($\lambda = 0.15418$ nm), β is the full-width at half-maximum (FWHM) of main intensity peak and θ is the angle of diffraction [46]. The mean size of the crystallites in HMgO structure which was found by the FWHM of the XRD peak (101) by Eq. (12). The crystallite size was estimated to be 3.42 nm. The surface chemistry and functional groups of adsorbents have an undeniable role in the adsorptive removal of adsorbate molecules. Fig. 2(c) shows the FTIR spectrum of HMgO in the range of 500–4,000 cm⁻¹. For HMgO nanoparticles, the characteristic peaks found at 1,433 and 3,698 cm⁻¹ related to hydrogen-bonded OH, 434 cm⁻¹ related to magnesium oxygen bond vibrations (Mg–O), 1,641 and 3,441 cm⁻¹ were corresponded to H–O–H stretching. Finally, the band appeared at 3,698 cm⁻¹ can be attributed to the stretching and bending vibrational frequencies of HMgO bending. The band appeared at 3,698 cm⁻¹ is eliminated, if nanoparticles are

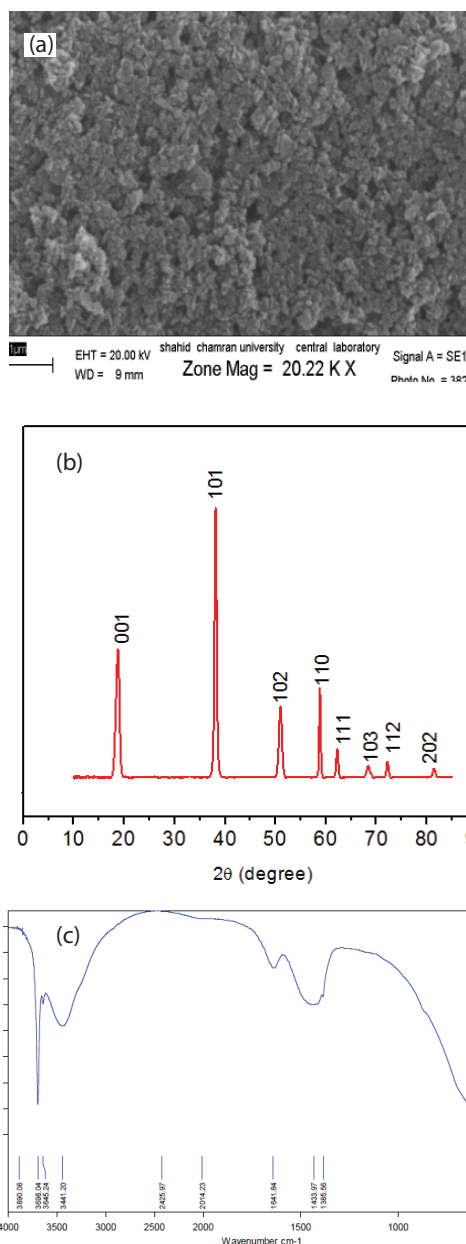


Fig. 2. SEM image (a), XRD spectra (b) and FTIR spectra (c) of sample of HMgO nanoparticles.

heated for 2 h at 400°C. This reflects the magnesium hydroxide with hexagonal structure convert to the magnesium oxide with cubic structure.

3.2. Effect of initial pH and point of zero charge

Solution pH has always been considered as a critical factor in a typical batch system, due, in essence, to its significant effect on the charges of the adsorbent surfaces [15,47]. BPA removal from aqueous solution was carried out at various pH values of 4, 7, 9 and 11 by micro-additions of adding diluted HCl or NaOH, while the other experimental factors were 50 min contact time, 10 mg/L BPA concentration and 20 mg/L HMgO dosage. The obtained findings are

demonstrated in Fig. 3, indicating no significant changes in BPA adsorptive removal with enhancing solution pH from 4 to 7. However, further increase in solution pH to 9, caused a slight increase in BPA adsorption. While, by increasing pH to 11, the adsorption efficiency of BPA witnessed a decline from 4.2 to 2.5 mg/g. To explain the adsorption rate onto HMgO nanoparticles, BPA has a pK_a value of 10.6. At pH values $pH < 9$ and $9-12$, BPA is appeared in molecular and anionic statuses ($HBPA^-$ or as BPA^{2-}), respectively [15]. On the other hand, the point of zero charge (pzc) was studied to investigate the surface charge of HMgO. The pzc of HMgO is 8 which means that the surface of HMgO carrying positive charges below pH 8 and surface of HMgO will be deprotonated at pH values higher than 8. With an increase in pH from 9 to 11, the number of hydroxyl ions in the solution has high competition with $HBPA^-$ or BPA^{2-} to occupy the vacant surface reactive sites of adsorbent.

3.3. Effect of adsorbent dosage

BPA adsorptive removal was studied at different dosages of applied nanoparticles (2, 5, 10, 20, 50 and 100 mg/L, reaction time of 50 min, initial BPA concentration of 10 mg/L, pH of 7.0) and the related findings are illustrated in Fig. 4. Accordingly, a simultaneous improvement in BPA adsorptive removal (24.9%–100%), Fig. 4, and decrease in adsorbed BPA (13 to 1 mg/g), Fig. 4, were observed by enhancement of adsorbent dosage from 2 to 100 mg/L. The increase in the BPA removal efficiency (%) at high adsorbent dosages is due to the increasing available surface area and subsequently more adsorptive sites in the adsorption process. On the other hand, increasing the quantity of adsorbent dosage from 2 to 100 mg/L, resulted in decreasing the amount of adsorbed pollutant per unit of the adsorbent dosage, because of the fact that a few number of active sites are remained unoccupied [47,49]. According to Fig. 4, increasing the adsorbent dosage from 50 to 100 mg/L, the removal percentage of BPA by the adsorbent represented an insignificant increase. Therefore, 20 mg/L was selected as an equilibrium amount of adsorbent in the next batch experiments. Similar findings have been reported by Noorimotlagh et al. [49] and Kumar and Porkodi [51].

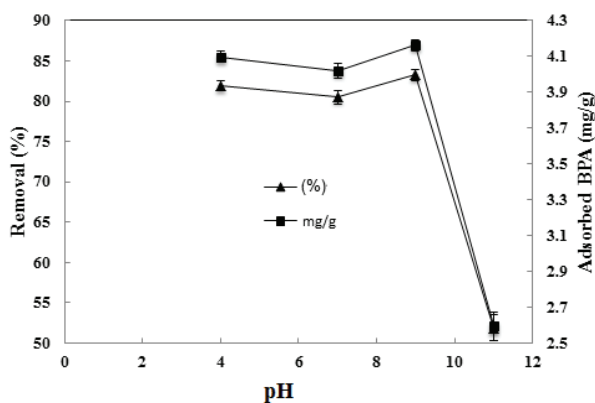


Fig. 3. Variations in the amount of adsorbed BPA onto HMgO nanoparticles vs. initial pH.

3.4. Effect of contact time and kinetics study

Fig. 5 shows the effect of reaction time at six different intervals (5, 10, 20, 50, 100 and 200 min) at adsorbent dosage of 20 mg/L, initial BPA concentration of 10 mg/L, pH of 7.0. BPA adsorptive removal showed a significant enhancement to 80%, by passing the reaction time to approximately 50 min. Afterwards, a slight increase was seen in the removal efficiency of BPA from 80% to 90%, with increasing contact time from 50 to 100 min which became constant at 200 min. This issue can be illustrated by the fact that at the first stages of reaction, the large number of vacant surface reactive sites tends to adsorb more adsorbate molecules. Afterwards, the majority of active sites present on the surface of the HMgO nanoparticles are saturated by the adsorbate molecules. Thus, the contact time of 50 min was selected as an equilibrium time for conducting subsequent experimental runs. The adsorption rate is known as an effective agent beneficial for the evaluation of adsorption mechanism in order to obtain the essential information for sketching and modeling of the experimental process [48]. Thus, the linear forms of the pseudo-first-order and pseudo-second-order kinetics models were applied for fitting the experimental data of BPA removal. The parameters of pseudo-first-order and pseudo-second-order models were also obtained. Results of the present research

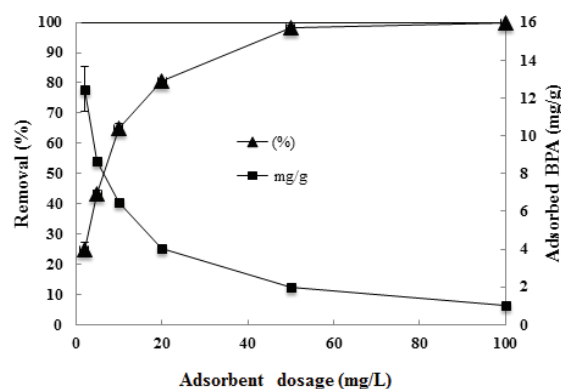


Fig. 4. Effect of adsorbent dosage on the amount of adsorbed BPA (mg/g) and removal efficiency (%) of BPA.

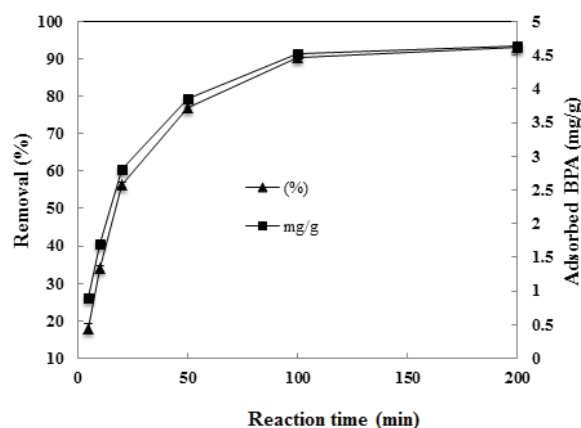


Fig. 5. Effect of contact time on the adsorption of BPA.

showed that the adsorption kinetics of BPA onto the HMgO nanoparticles followed the pseudo-first-order kinetics model. Pseudo-first-order model (0.998) had higher coefficient of correlation than pseudo-second-order model (0.997). In pseudo-first-order kinetics model, there was a good agreement between the experimental and calculated values of q_e (q_e cal. = 4.2 mg/g and q_e exp. = 3.85 mg/g), while the experimental and calculated values of q_e for pseudo-first-order kinetics model were q_e cal. = 5.15 mg/g and q_e exp. = 3.85 mg/g, respectively. Yusuf and Shehu reported similar results for BPA, 17β-estradiol and 17α-ethinylestradiol sorption onto powdered poly-1-methylperrol-2-ylsquaraine [52].

3.5. Effect of initial concentration of BPA and isotherm study

The initial concentration of contaminants is known as an effective parameter on the sorption process [49]. Fig. 6 depicts the adsorptive removal of BPA from aqueous solution at nine different amounts of contaminant (2, 5, 10, 20, 50, 100, 200, 250 and 309 mg/L) at the adsorbent dosage of 20 mg/L, the reaction time of 50 min and pH of 7.0. It is observed that with an enhancement in the initial BPA concentration from 2 to 309 mg/L, the amount of BPA adsorbed per HMgO nanoparticles mass unit was increased (from 0.34 to 46.4 mg/g). It can be stated that because of the strong driving force, decreased resistance to the uptake of BPA molecules on adsorbent surface, between the aqueous solution and HMgO nanoparticles as solid phase that occurs by increasing the initial concentration of the adsorbates and consequently the adsorption capacity increases [47,48]. Moreover, the better elucidation of the adsorption behavior

with different adsorbents is the study of adsorption isotherms. Adsorption isotherm is a critical factor in describing the adsorption process. The isotherm parameters of Freundlich, Langmuir, D–R, R–P, Temkin and Langmuir–Freundlich models are tabulated in Table 1. Based on Table 1, the coefficients of correlation (R^2) of Freundlich were high, compared with the other five models. Thus, the isotherm data were better fitted to Freundlich model for describing the adsorption mechanism that took place between HMgO and BPA ions [24]. In another study, Li et al. stated that the findings of BPA sorption have a significant correlation with Freundlich model which are in line with the obtained findings of this research [53].

3.6. Regeneration of HMgO

The process of adsorbent regeneration is an important issue influencing on the adsorption process expenses and consequently reusing adsorbents and recovery of adsorbate [12,48]. The regeneration experiments were performed by means of methanol and dichloromethane for determination of the efficiency of the spent sorbent. To perform regeneration of adsorbent, some experiments were performed at an initial BPA concentration of 10 mg/L, adsorbent dosage of 20 mg/L and reaction time of 50 min. Table 2 shows the results of BPA adsorptive removal using pristine and regenerated HMgO nanoparticles. Eq. (11) was applied for estimation of the regeneration efficiency (R_e) as follows:

$$R_e = \frac{M_{ac}}{M_{bc}} \times 100 \tag{11}$$

where M_{bc} and M_{ac} (mg/g) are the amounts of adsorbed BPA onto HMgO nanoparticles before and after regeneration tests, respectively [47]. As can be seen, the regeneration

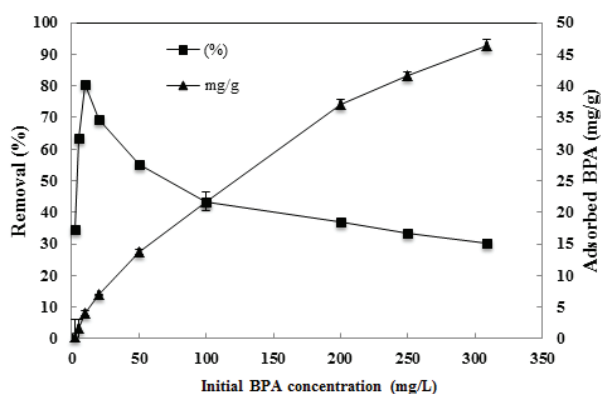


Fig. 6. Effect of initial BPA concentration on the HMgO nanoparticles.

Table 2
The results of regeneration test

Adsorbent	First step		Second step		Third step	
	η (%)	R_e (%)	η (%)	R_e (%)	η (%)	R_e (%)
HMgO (methanol)	80.51	95.95	79.43	94.52	92.14	77.24
HMgO (dichloro-methane)	81.2	96.42	76.2	90.71	82.61	69.8
HMgO (virgin)	85.33	–	85.33	–	–	85.33

Table 1
Isotherm models for the adsorption of BPA onto HMgO nanoparticles

Langmuir isotherm model	Freundlich isotherm model	Dubinini–Radushkevich (D–R) isotherm model	Redlich–Peterson (R–P) isotherm model	Temkin isotherm model	Langmuir–Freundlich isotherm model						
R^2	0.958	R^2	0.997	R^2	0.994	R^2	0.996	R^2	0.935	R^2	0.918
q_{max} (mg/g)	62.5	K_f (mg/g)	2.55	β	-5×10^{-9}	β	0.456	b	11.37	b	0.036
K (L/mg)	0.013	n	1.84	q_m (mol/g)	9×10^{-10}	a_R (mg/g)	391	K_t	-18.09	n	0.956
						K_R (L/g)	998			q_m	0.956

via methanol and dichloromethane (200 μL for 50 min with 200 rpm) was the most suitable approach to desorb BPA from HMgO. Results of regeneration experiments revealed that the rate of regeneration (%) by methanol and dichloromethane showed a declining trend from 80.51% to 77.24% and 81.2% to 69.8%, respectively, after three consecutive cycles. Hence, from the findings of regeneration tests, it can be postulated that methanol could effectively regenerate HMgO nanoparticles occupied by BPA molecules.

4. Conclusions

This research showed that HMgO nanoparticles are efficient agents for adsorption of BPA, one of EDCs, from aqueous solutions. HMgO nanoparticle was synthesized via sol-gel process using [BMIM] BF_4^- ionic liquid and after characterization by SEM, XRD and FTIR techniques was used as a sorbent for investigation of BPA adsorptive removal. Results of X-ray diffraction showed that HMgO nanoparticles were successfully synthesized and illustrated high purity and crystallinity. The average crystallite and nanoparticle size were 3.42 (according to Debye-Scherrer's formula) and ranging from 20 to 80 nm (according to SEM), respectively. BPA adsorptive removal via the applied adsorbent was highly influenced by solution pH, contact time, adsorbent dosage and BPA concentration. The optimum solution pH and adsorbent dosage were achieved at 7 and 20 mg/L, respectively. The optimum reaction time and adsorption capacity of BPA adsorptive removal using HMgO nanoparticles were obtained 50 min and 4.2 mg/g, respectively. Findings indicated that Freundlich isotherm ($R^2 = 0.997$) and pseudo-first-order kinetic ($R^2 = 0.998$) models showed the best-fitted with data of BPA removal, in comparison with the other models. Overall, HMgO nanoparticles were the efficient adsorbents for treating BPA-contaminated media.

Acknowledgments

The authors wish to acknowledge the financial and academic assistance of the deputy of research affairs Ahvaz Jundishapur University of Medical Sciences, as the part of the Parvaneh Bahrami thesis with the reference number of ETRC 9113.

References

- [1] Z. Noorimotlagh, G. Shams Khoramabadi, R. Darvishi, The application of ZnO/SiO₂ nanocomposite for the photocatalytic degradation of a textile dye in aqueous solutions in comparison with pure ZnO nanoparticles, *Desal. Wat. Treat.*, 56 (2015) 2551–2558.
- [2] J. Kwon, B. Lee, Bisphenol A adsorption using reduced graphene oxide prepared by physical and chemical reduction methods, *Chem. Eng. Res. Des.*, 104 (2015) 519–529.
- [3] N. Jaafarzadeh, B. Kakavandi, A. Takdastan, R.R. Kalantary, M. Azizi, S. Jorfi, Powder activated carbon/Fe₃O₄ hybrid composite as a highly efficient heterogeneous catalyst for Fenton oxidation of tetracycline: degradation mechanism and kinetic, *RSC Adv.*, 5 (2015) 84718–84728.
- [4] M. Ahmadi, H.R. Motlagh, N. Jaafarzadeh, A. Mostoufi, R. Saeedi, G. Barzegar, S. Jorfi, Enhanced photocatalytic degradation of tetracycline and real pharmaceutical wastewater using MWCNT/TiO₂ nano-composite, *J. Environ. Manage.*, 186 (2017) 55–63.
- [5] N. Jaafarzadeh, H. Amiri, M. Ahmadi, Factorial experimental design application in modification of volcanic ash as a natural adsorbent with Fenton process for arsenic removal, *Environ. Technol.*, 33 (2012) 159–165.
- [6] A.A. Babaei, Z. Baboli, N. Jaafarzadeh, G. Goudarzi, M. Bahrami, M. Ahmadi, Synthesis, performance, and nonlinear modeling of modified nano-sized magnetite for removal of Cr(VI) from aqueous solutions, *Desal. Wat. Treat.*, 53 (2015) 768–777.
- [7] M. Rastegari Mehr, B. Keshavarzi, F. Moore, E. Sacchi, A.R. Lahijanzadeh, S. Eydivand, N. Jaafarzadeh, S. Naserian, M. Setti, S. Rostami, Contamination level and human health hazard assessment of heavy metals and polycyclic aromatic hydrocarbons (PAHs) in street dust deposited in Mahshahr, southwest of Iran, *Hum. Ecol. Risk Assess. Int. J.*, 22 (2016) 1726–1748.
- [8] S. Salehinia, S.M. Ghoreishi, F. Maya, V. Cerdà, Hydrophobic magnetic montmorillonite composite material for the efficient adsorption and microextraction of bisphenol A from water samples, *J. Environ. Chem. Eng.*, 4 (2016) 4062–4071.
- [9] A. Bhatnagar, I. Anastopoulos, Adsorptive removal of bisphenol a (BPA) from aqueous solution: a review, *Chemosphere*, 168 (2017) 885–902.
- [10] Z. Noorimotlagh, S.A. Mirzaee, M. Ahmadi, N. Jaafarzadeh, F. Rahim, The possible DNA damage induced by environmental organic compounds: the case of Nonylphenol, *Ecotoxicol. Environ. Saf.*, 158 (2018) 171–181.
- [11] Z. Noorimotlagh, I. Kazeminezhad, N. Jaafarzadeh, M. Ahmadi, Z. Ramezani, S.S. Martinez, The visible-light photodegradation of nonylphenol in the presence of carbon-doped TiO₂ with rutile/anatase ratio coated on GAC: effect of parameters and degradation mechanism, *J. Hazard. Mater.*, 350 (2018) 108–120.
- [12] A.C. Arampatzidou, E.A. Deliyanni, Comparison of activation media and pyrolysis temperature for activated carbons development by pyrolysis of potato peels for effective adsorption of endocrine disruptor bisphenol-A, *J. Colloid Interface Sci.*, 466 (2016) 101–112.
- [13] X. Tan, Y. Wan, Y. Huang, C. He, Z. Zhang, Z. He, L. Hu, J. Zeng, D. Shu, Three-dimensional MnO₂ porous hollow microspheres for enhanced activity as ozonation catalysts in degradation of bisphenol A, *J. Hazard. Mater.*, 321 (2017) 162–172.
- [14] J.R. Koduru, L.P. Lingamdinne, J. Singh, K.-H. Choo, Effective removal of bisphenol A (BPA) from water using a goethite/activated carbon composite, *Process Saf. Environ. Prot.*, 103 (2016) 87–96.
- [15] S. Bele, V. Samanidou, E. Deliyanni, Effect of the reduction degree of graphene oxide on the adsorption of Bisphenol A, *Chem. Eng. Res. Des.*, 109 (2016) 573–585.
- [16] R.E. Morrissey, J.D. George, C.J. Price, R.W. Tyl, M.C. Marr, C.A. Kimmel, The developmental toxicity of bisphenol A in rats and mice, *Fundam. Appl. Toxicol.*, 8 (1987) 571–582.
- [17] C.A. Staples, P.B. Dome, G.M. Klecka, S.T. Oblock, L.R. Harris, A review of the environmental fate, effects, and exposures of bisphenol A, *Chemosphere*, 36 (1998) 2149–2173.
- [18] R.E. Chapin, J. Adams, K. Boekelheide, L.E. Gray, S.W. Hayward, P.S.J. Lees, B.S. McIntyre, K.M. Portier, T.M. Schnorr, S.G. Selevan, NTP-CERHR expert panel report on the reproductive and developmental toxicity of bisphenol A, *Birth Defects Res. B Dev. Reprod. Toxicol.*, 83 (2008) 157–395.
- [19] D.B. Pickford, M.J. Hetheridge, J.E. Caunter, A.T. Hall, T.H. Hutchinson, Assessing chronic toxicity of bisphenol A to larvae of the African clawed frog (*Xenopus laevis*) in a flow-through exposure system, *Chemosphere*, 53 (2003) 223–235.
- [20] H.C. Alexander, D.C. Dill, L.W. Smith, P.D. Guiney, P. Dorn, Bisphenol A: acute aquatic toxicity, *Environ. Toxicol. Chem.*, 7 (1988) 19–26.
- [21] M. Chen, M. Ike, M. Fujita, Acute toxicity, mutagenicity, and estrogenicity of bisphenol-A and other bisphenols, *Environ. Toxicol.*, 17 (2002) 80–86.
- [22] M. Ema, S. Fujii, M. Furukawa, M. Kiguchi, T. Ikka, A. Harazono, Rat two-generation reproductive toxicity study of bisphenol A, *Reprod. Toxicol.*, 15 (2001) 505–523.
- [23] Z. Noorimotlagh, N. Jaafarzadeh, M. Ahmadimoghadam, F. Rahim, An updated systematic review on the possible effect of

- nonylphenol on male fertility, *Environ. Sci. Pollut. Res. Int.*, 24 (2017) 3298–3314.
- [24] N. Abdullah, R.J. Gohari, N. Yusof, A.F. Ismail, J. Juhana, W.J. Lau, T. Matsuura, Polysulfone/hydrous ferric oxide ultrafiltration mixed matrix membrane: preparation, characterization and its adsorptive removal of lead (II) from aqueous solution, *Chem. Eng. J.*, 289 (2016) 28–37.
- [25] M. Heidarizad, S.S. Şengör, Synthesis of graphene oxide/magnesium oxide nanocomposites with high-rate adsorption of methylene blue, *J. Mol. Liq.*, 224 (2016) 607–617.
- [26] M. Naushad, A. Mittal, M. Rathore, V. Gupta, Ion-exchange kinetic studies for Cd(II), Co(II), Cu(II), and Pb(II) metal ions over a composite cation exchanger, *Desal. Wat. Treat.*, 54 (2015) 2883–2890.
- [27] G. Sharma, M. Naushad, D. Pathania, A. Mittal, G.E. El-Desoky, Modification of *Hibiscus cannabinus* fiber by graft copolymerization: application for dye removal, *Desal. Wat. Treat.*, 54 (2015) 3114–3121.
- [28] A. Mittal, J. Mittal, Hen Feather: A Remarkable Adsorbent for Dye Removal, *Green Chemistry for Dyes Removal from Wastewater: Research Trends and Applications*, Wiley Online Library, 2015, pp. 409–457.
- [29] A. Mittal, M. Teotia, R.K. Soni, J. Mittal, Applications of egg shell and egg shell membrane as adsorbents: a review, *J. Mol. Liq.*, 223 (2016) 376–387.
- [30] A. Mittal, R. Ahmad, I. Hasan, Biosorption of Pb²⁺, Ni²⁺ and Cu²⁺ ions from aqueous solutions by L-cystein-modified montmorillonite-immobilized alginate nanocomposite, *Desal. Wat. Treat.*, 57 (2016) 17790–17807.
- [31] A. Mittal, R. Ahmad, I. Hasan, Iron oxide-impregnated dextrin nanocomposite: synthesis and its application for the biosorption of Cr(VI) ions from aqueous solution, *Desal. Wat. Treat.*, 57 (2016) 15133–15145.
- [32] Z. Noorimotlagh, S. Shahriyar, R. Darvishi Cheshmeh Soltani, R. Tajik, Optimized adsorption of 4-chlorophenol onto activated carbon derived from milk vetch utilizing response surface methodology, *Desal. Wat. Treat.*, 57 (2016) 14213–14226.
- [33] A. Mittal, Retrospection of Bhopal gas tragedy, *Toxicol. Environ. Chem.*, 98 (2016) 1079–1083.
- [34] R. Ahmad, I. Hasan, A. Mittal, Adsorption of Cr (VI) and Cd (II) on chitosan grafted polyaniline-OMMT nanocomposite: isotherms, kinetics and thermodynamics studies, *Desal. Wat. Treat.*, 58 (2017) 144–153.
- [35] M.Y. Nassar, T.Y. Mohamed, I.S. Ahmed, I. Samir, MgO nanostructure via a sol-gel combustion synthesis method using different fuels: an efficient nano-adsorbent for the removal of some anionic textile dyes, *J. Mol. Liq.*, 225 (2017) 730–740.
- [36] H.M. Moghaddam, H. Beitollahi, S. Tajik, M. Malakootian, H.K. Maleh, Simultaneous determination of hydroxylamine and phenol using a nanostructure-based electrochemical sensor, *Environ. Monit. Assess.*, 186 (2014) 7431–7441.
- [37] R.D.C. Soltani, G.S. Khorramabadi, A.R. Khataee, S. Jorfi, Silica nanopowders/alginate composite for adsorption of lead (II) ions in aqueous solutions, *J. Taiwan Inst. Chem. Eng.*, 45 (2014) 973–980.
- [38] A. Mittal, R. Ahmad, I. Hasan, Poly (methyl methacrylate)-grafted alginate/Fe₃O₄ nanocomposite: synthesis and its application for the removal of heavy metal ions, *Desal. Wat. Treat.*, 57 (2016) 19820–19833.
- [39] A. Mittal, M. Naushad, G. Sharma, Z.A. AlOthman, S.M. Wabaidur, M. Alam, Fabrication of MWCNTs/ThO₂ nanocomposite and its adsorption behavior for the removal of Pb(II) metal from aqueous medium, *Desal. Wat. Treat.*, 57 (2016) 21863–21869.
- [40] V. Srivastava, Y.C. Sharma, M. Sillanpää, Green synthesis of magnesium oxide nanoflower and its application for the removal of divalent metallic species from synthetic wastewater, *Ceram. Int.*, 41 (2015) 6702–6709.
- [41] K. Umar, M.M. Haque, M. Muneer, T. Harada, M. Matsumura, Mo, Mn and La doped TiO₂: synthesis, characterization and photocatalytic activity for the decolorization of three different chromophoric dyes, *J. Alloys Compd.*, 578 (2013) 431–438.
- [42] M. Crişan, N. Drăgan, D. Crişan, A. Ianculescu, I. Niţoi, P. Oancea, L. Todan, C. Stan, N. Stănică, The effects of Fe, Co and Ni dopants on TiO₂ structure of sol-gel nanopowders used as photocatalysts for environmental protection: a comparative study, *Ceram. Int.*, 42 (2016) 3088–3095.
- [43] M. Sundrarajan, R.G.R. Gandhi, J. Suresh, S. Selvam, S. Gowri, Sol-gel synthesis of MgO nanoparticles using ionic liquid-[BMIM] BF₄⁻ as capping agent, *Nanosci. Nanotechnol. Lett.*, 4 (2012) 100–104.
- [44] S.D. Meenakshi, M. Rajarajan, S. Rajendran, Z.R. Kennedy, G. Brindha, Synthesis and characterization of magnesium oxide nanoparticles, *Elixir Nanotechnol.*, 50 (2012) 10618–10620.
- [45] J.S. Piccin, G.L. Dotto, L.A.A. Pinto, Adsorption isotherms and thermochemical data of FD&C Red n° 40 binding by chitosan, *Braz. J. Chem. Eng.*, 28 (2011) 295–304.
- [46] Q. Chen, H. Liu, Y. Xin, X. Cheng, TiO₂ nanobelts – effect of calcination temperature on optical, photoelectrochemical and photocatalytic properties, *Electrochim. Acta*, 111 (2013) 284–291.
- [47] Z. Noorimotlagh, R.D.C. Soltani, A.R. Khataee, S. Shahriyar, H. Nourmoradi, Adsorption of a textile dye in aqueous phase using mesoporous activated carbon prepared from Iranian milk vetch, *J. Taiwan Inst. Chem. Eng.*, 45 (2014) 1783–1791.
- [48] H. Nourmoradi, A.R. Ghiasvand, Z. Noorimotlagh, Removal of methylene blue and acid orange 7 from aqueous solutions by activated carbon coated with zinc oxide (ZnO) nanoparticles: equilibrium, kinetic, and thermodynamic study, *Desal. Wat. Treat.*, 55 (2015) 252–262.
- [49] Z. Noorimotlagh, R. Darvishi Cheshmeh Soltani, G. Shams Khorramabadi, H. Godini, M. Almasian, Performance of wastewater sludge modified with zinc oxide nanoparticles in the removal of methylene blue from aqueous solutions, *Desal. Wat. Treat.*, 57 (2016) 1684–1692.
- [50] S. Jorfi, R.D.C. Soltani, M. Ahmadi, A. Khataee, M. Safari, Sono-assisted adsorption of a textile dye on milk vetch-derived charcoal supported by silica nanopowder, *J. Environ. Manage.*, 187 (2017) 111–121.
- [51] K.V. Kumar, K. Porkodi, Mass transfer, kinetics and equilibrium studies for the biosorption of methylene blue using *Paspalum notatum*, *J. Hazard. Mater.*, 146 (2007) 214–226.
- [52] M.K. Yusuf, M.S. Shehu, Kinetic modeling and equilibrium studies of selected endocrine disrupting chemicals on to low cost adsorbent, *Adv. Appl. Sci. Res.*, 4 (2013) 331–341.
- [53] Z. Li, M.A. Gondal, Z.H. Yamani, Preparation of magnetic separable CoFe₂O₄/PAC composite and the adsorption of bisphenol A from aqueous solution, *J. Saudi Chem. Soc.*, 18 (2014) 208–213.